FULL PAPER

Photoresponsive Protein–Graphene–Protein Hybrid Capsules with Dual Targeted Heat-Triggered Drug Delivery Approach for Enhanced Tumor Therapy

*Shang-Hsiu Hu, Ren-Hong Fang, Yu-Wei Chen, Bang-Jie Liao, I-Wei Chen, and San-Yuan Chen**

A novel photo-responsive protein–graphene–protein (PGP) capsule that doubles as a photothermal agent with core/shell structure is constructed by anchoring reduced graphene oxide nanosheets on one-component protein (lactoferrin) shell through a double emulsion method. PGP capsules can transport fully concealed hydrophilic anticancer cargo, doxorubicin (Dox), with a large payload (9.43 μmol g^{-1}) to be later unloaded in a burst-like manner by photo-actuation triggered by near-infrared irradiation. Being biocompatible yet with a high cancer cell targeting efficiency, PGP capsules have successfully eradicated subcutaneous tumors in 10 d following a single 5 min NIR irradiation without distal damage. Besides, the photochemothermal therapy of PGP capsules eradicates tumor cells not only in the light-treating area but also widely light-omitted tumor cells, overcoming the tumor recurrence due to efficient cell killing efficacy. These results demonstrate that the PGP capsule is a potential new drug delivery platform for local-targeting, on-demand, photoresponsive, combined chemotherapy/hyperthermia for tumor treatment and other biomedical applications.

1. Introduction

Locally-triggered-release nanosystems (iron oxide particle, gold, and graphene) have seen remarkable use in the near infrared (NIR) photothermal destruction of tumors. However, photothermal therapy alone is unlikely to eradicate malignant cells at once because of the locally heterogeneous distribution of heat in the tumor.[1–6] Therefore, it is highly desirable to combine photothermal ablation therapy with chemotherapy to enhance the therapeutic efficacy. Chemotherapy, the most common treatment for many cancers, however, is known to cause severe problems such as drug resistance and toxic side effect due to non-specific distribution of anti-cancer drugs. One approach to mitigate the side effect is to use targeted delivery systems to conceal the drug until they approach the tumor.[7,8] A stimuli-responsive targeted drug-carrier that can combine physical (photothermal) therapy together with on-demand drug release of a high local concentration spread to cover a large treatment area is the key to achieve success in killing the entire cancer cell population.

These difficulties are fundamentally related to materials issue and challenges on the drugs sealing and on-demand releasing. Despite most locally-triggered-release nanosystems (iron oxide particle, gold, and graphene) being able to rapidly release the cargo under the treatment, the cargo (including gene and anti-cancer drugs) is typically left tethered to or adsorbed onto the outer surfaces of the carriers.[9–13] Therefore, premature release of the cargo before it reaches the target site and unintended side effects may be unavoidable. Furthermore, owing to low drug dosage adsorption on the carriers, the accumulation of drugs probably cannot reach the therapeutic window, and so further affect surrounding cancer cells around the treating area. Another example is the water-in-oil-in-water (W/O/W) nanoparticle which is a popular construction for encapsulating and delivering high dosages of drugs.[14–17] It has a small water-like core within an oil-like shell that is stabilized by an amphipathic surfactant.[18,19] However, such particles are typically stabilized by multiple surfactants during a two-step emulsifying procedure, which inevitably adds processing complexity and may raise potential toxicity concerns for in vivo biomedical applications. The drug molecules encapsulated in the watery core may diffuse out owing to the structure loose of polymer shell. Therefore, natural drug release from the core that can be manipulated by the shell is highly desirable.

Here we propose a new protein–graphene–protein (PGP) platform for targeted and enhanced drug delivery with on-demand drug release of high concentrations, using a new family of water-in-oil-in-wall (W/O/W) core–shell nanocapsules

Prof. S.-H. Hu, Dr. R.-H. Fang
Department of Biomedical Engineering
and Environmental Sciences
National Tsing Hua University
Hsinchu 300, Taiwan
Dr. Y.-W. Chen, Dr. B.-J. Liao, Prof. S.-Y. Chen
Department of Materials Science and Engineering
National Chiao Tung University
Hsinchu 300, Taiwan
E-mail: sanyuanchen@mail.nctu.edu.tw
Prof. I-W. Chen
Department of Materials Science and Engineering
University of Pennsylvania
Philadelphia, PA 19104–6272, USA

DOI: 10.1002/adfm.201400080

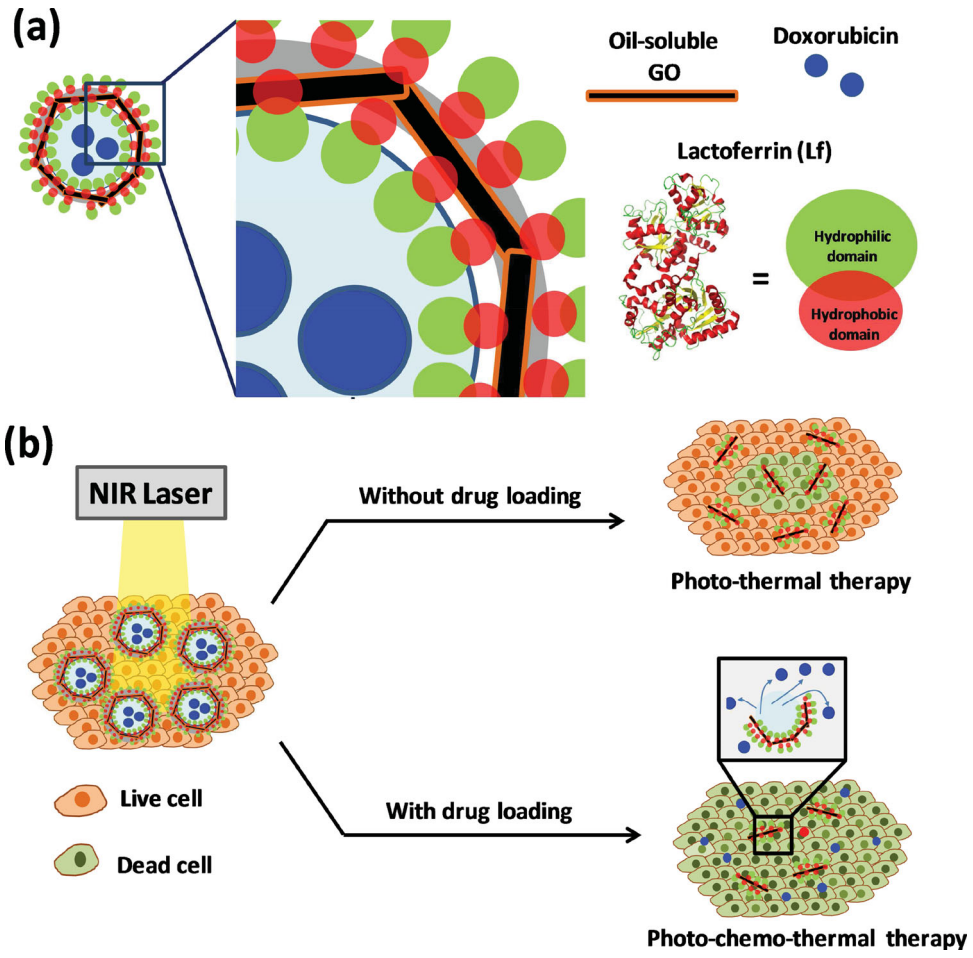

Figure 1. Schematic illustration of: a) core–shell protein–graphene–protein (PGP) capsules encapsulating hydrophilic doxorubicin; and, b) under NIR irradiation, the PGP capsules with and without loading drug exhibit different cell killing efficacy; combining thermo- and chemotherapy, the PGP capsules can eradicate cancer cells extensively.

made from the self assembly of a one-component targeting protein and reduced graphene oxide (rGO) nanosheets (**Figure 1**a). In this approach, the protein constitutes the shell and serves as the surfactant (with potential targeting functions); the rGO stabilizes the shell to minimize unintended drug leakage because of the strong paper-like structure, but it also serves as the sensor/actuator that triggers drug release. To achieve these goals, we selected a biocompatible protein (lactoferrin, Lf)),[20–22] since it has a suitable hydrophobic/hydrophilic property to serve the above functionality that is critical for the synthetic scheme of the core–shell structure during self-assembly. Our choice of incorporating protein as a structural element of the drug delivery vehicle is partially motivated by the following consideration. Nanoparticles are known to elicit serum proteins as a coating when they are in circulation, which typically lead to enhanced uptake of nanoparticles by macrophages. As a result, nanoparticles are lost and no longer available to tumor. Currently, the most common approach to prevent this from happening is to use a polyethylene glycol (PEG) coating. However, coating proteins appear on many natural nanoparticles, such as apolipoproteins on lipoproteins which can also reduce the occurrence of uptake by macrophages. Therefore, it is theoretically possible to incorporate proteins as a design coating in the nanoparticle structure to prevent unintended serum protein coating. The PGP capsule is a first attempt to this approach to designed nanoparticles with enhanced functionality. Moreover, compared to other rGO composites, the core–shell capsules carrying a high payload of hydrophilic drug (doxorubicin, Dox) in the core display little drug release until it is triggered by NIR. Since NIR-responsive rGO can induce local heating, both photochemotherapy and photothermal therapy contribute to cell kill and tumor treatment synergistically, actuating a locally large-dosage of Dox release with enhanced permeability to spread and to eradicate wide-ranged malignant cells omitted by light, as shown in Figure 1b. Therefore, the PGP capsule is considered as an excellent new delivery platform for on-demand, enhanced chemotherapy/hyperthermia for deep tumor therapy.

2. Results and Discussion

2.1. Synthesis and Characterization of PGP Capsules

The core–shell PGP capsules were synthesized from an emulsifying process, which includes: a) lactoferrin as both a shell

constituent and the surfactant, and, b) oil-soluble rGO as the shell stabilizer. To ascertain the emulsifying ability of Lf, screening tests were first conducted by measuring the hydrophilic–lipophilic balance (HLB) value of Lf, as described in Figure S1 (see the Supporting Information). The results found the HLB of Lf ranging from 4 to 10, indicating that it is a good candidate for stabilizing both water-in-oil (W/O) and oil-in-water (O/W) emulsions. The result is also consistent with several recent studies in which other proteins were used to form micelles or lipoproteins around a hydrophobic drug, displaying good amphiphatic properties.[23,24]

The synthetic procedure of the PGP capsules is schematically illustrated in **Figure 2**a. In the first step, an aqueous emulsion of hydrophilic compounds (in this study water-soluble quantum dots and doxorubicin) is emulsified, using Lf as the surfactant, with the superhydrophobic rGO synthesized by octadeylamine (ODA) modification.[25] To co-localize the rGO in the hydrophobic interlayer of Lf, only small sizes of rGO from 60 to 110 nm were used in this preparation (the ultrasmall sizes of rGO were separated by centrifugation technique at 17 000 rpm and measured by dynamic light scattering in Figure S2, see the Supporting Information). In the second step of the W/O/W double emulsion, the organic solvent is emulsified in a water continuous phase with Lf as the surfactant again. Due to the amphiphilic nature of Lf, a core–shell structure self-assembles tightly at the water–oil interface with their lipophilic head groups of Lf in the shell oriented toward the hydrophobic rGO, which lies at the center of the shell sandwiched between Lf (i.e., a PGP shell, right illustration in Figure 2a). Finally, the organic phase was slowly evaporated leading to solidification of the shell. Here we used Lf as a model protein, but the rGO/protein capsules can also be fabricated by other amphiphilic biomoleculses such as transferrin, bovine serum albumin (BSA) or co-polypeptides (data not shown). Furthermore, rGO has been utilized previously in drug/gene delivery, cancer therapy, biosensing, bioimaging, and photothermal ablation.[26,27] Here, rGO is used as a structural element that also serves as an actuator for NIR-triggered drug release and photothermal therapy. NIR actuation is a very attractive mechanism and the potential for clinical uses due to its lower damage to living tissues and deeper penetration into tissues.[28,29]

To ascertain PGP capsule morphologies, dried W/O/W emulsion samples were examined by SEM (Figure 2b) and TEM (Figure 2c,d). Due to the nature of the emulsion approach, the particles are not absolutely monodisperse. As shown in the SEM image (Figure 2b), the PGP capsules have diameters ranging from 150 to 250 nm and show no observable crevices or cracks, implying a compatible interface between rGO and Lf. Under TEM (Figure 2c), the PGP capsules with inner hollow core and Lf-rGO composite shell can be clearly observed. The shell thickness is about 25 nm and no clear phase separation exists between two materials (Figure 2d). Due to the rGO present, the shell is much darker than the core compared to the pure organic polymer shell. Under the higher magnification of TEM, the QDs encapsulated in the PGP capsules can be clearly observed in Figure 2e. To further confirm the rGO in the shell, the Lf was removed by burning at 600 °C under Ar, which caused the remaining rGO to collapse, having a buckled and sphere-like appearance, as shown in Figure 2f. In the enlarged image, the compact QDs are still on the rGO (Figure 2g), revealing the high loading efficiency. The configurations of PGP capsules may be understood using the analogy of a balloon. A wet PGP capsules is like a water-filled balloon but after drying, the water escaped to cause a small hole on the surface (samples drying under vacuum). Since the Lf-rGO shell is relatively thick and reinforced by rGO, it is relatively rigid and capable of keeping a core–shell shape. Furthermore, it was noted that although protein is often applied as a surfactant to stabilize the interface of a O/W emulsion that contains an oily core made of another polymer or molecules (e.g., nutrients),[24] it by itself cannot form the emulsion without the assistance of rGO. Indeed, we found Lf did not yield any dry particles/capsules (mixing with water/chloroform, and then evaporating chloroform) but it simply precipitated into polymer-like crystals or thin films after drying. Only when hydrophobic rGO was added to the oil phase was it possible to form stable W/O/W emulsion with a Lf-rGO composite shell. The observation is reminiscent of liquid–liquid interface stabilization by colloidal particles, which is the so-called Pickering (solid-stabilized) emulsion process.[30–32] Therefore, the combined use of protein (Lf) and rGO as stabilizing nanosheets had made possible the discovery of Lf-rGO based double emulsion capsules for the first time. Furthermore, the UV-Vis spectra of PGP capsules and Dox-loaded PGP capsules (see Figure S3a,b of the Supporting Information) showed that there was no significant influence after loading Dox in PGP capsules. The surface charges of PGP capsules and Dox-loaded PGP capsules are –18.4 and –10.7 mV, respectively, as characterized by zeta potential (Zetasizer ZS90, Malvern Instruments Ltd, UK). Furthermore, the stability of PGP capsules was also evaluted during 4 °C storage in PBS solution and FBS-containing medium (see Figure S3c in the Supporting Information). The particle size distribution after 30 d was compared with that of the original, showing only slight coarsening of less than 6% (Figure S3c, Supporting Information). The size distribution of PGP capsules were also be investigated after 4 and 7 d at 37 °C under stirring conditions (Figure S3d, Supporting Information), exhibiting no obvious change. The magnetization curve after 30 d was also compared with that of the original, indicating less than 3% (Figure S3e, Supporting Information). The freeze-drying was also applied to preserve the PGP capsules (Figure S3f, Supporting Information). The dried product can be re-suspended in water, ant the re-suspended PGP capsules displayed similar size distribution as before.

2.2. Effects of rGO Concentrations on the Formation of PGP Capsules

Concerning rGO concentrations during the emulsifying processess, we found that the morphology of particle collapsed just like a deflated balloon after drying when the concentration of rGO decreased to 0.03 wt% (**Figure 3**a) because the amounts of rigid rGO were not enough to support the structure. Only when rGO is maintained at a suitable concentration (rGO of 0.15 wt%) can PGP capsules exist (Figure 3b). The mixture of PGP capsules and Lf-coated rGO can be observed when rGO is 0.3 wt% (Figure 3c). If further increasing the concentration, Lf-coated rGO particles were observed (Figure 3d) and no capsules

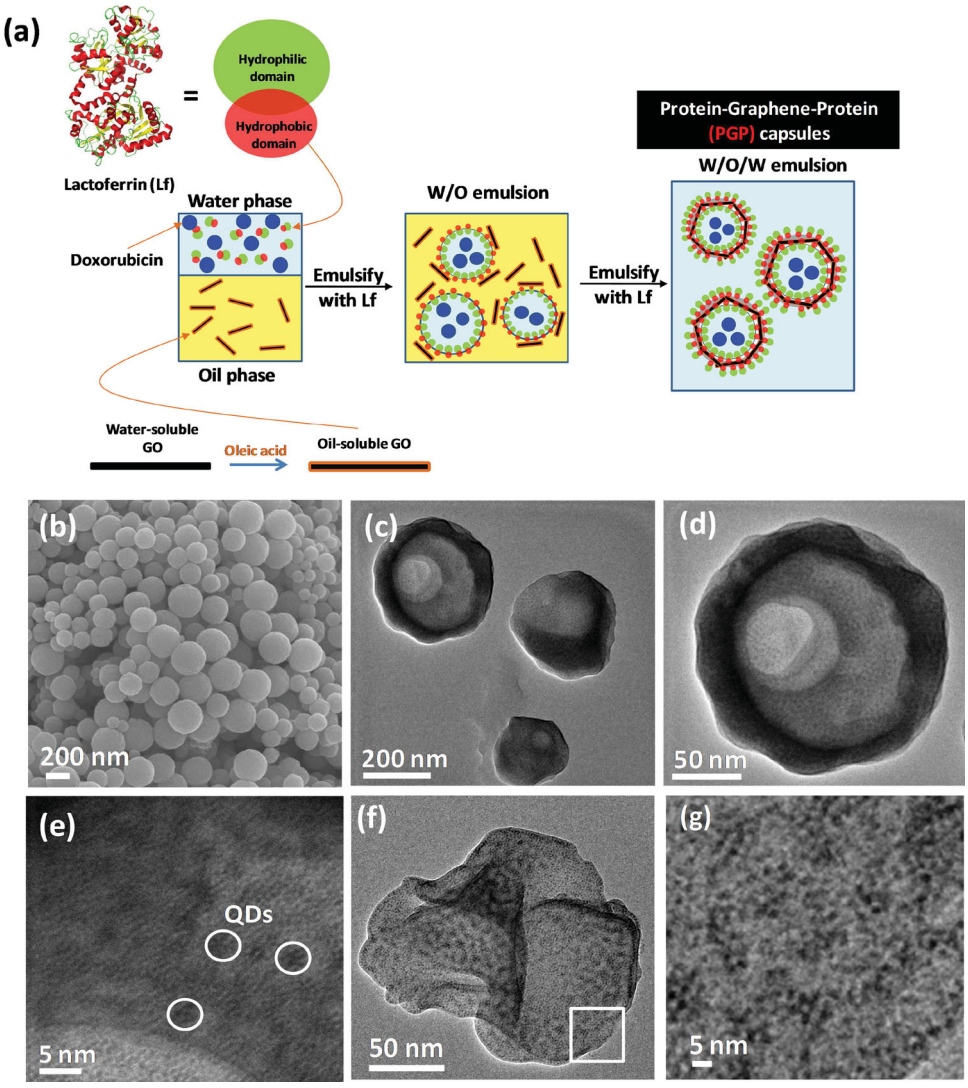

Figure 2. a) Schematic illustration of the key steps in protein–graphene–protein (PGP) capsule preparation: in the first step, aqueous solutions of Lf and Dox are emulsified in a volatile organic solvent containing oil-soluble rGO (W/O emulsion), followed by a second W/O/W emulsion with Lf as the surfactants again. b) SEM images, and, c,d) TEM images of PGP capsules at various magnifications. e) Under high magnification, the loaded quantum dots (QDs) can be observed in the PGP capsules. f,g) TEM images of PGP capsules after removing proteins: the capsules maintain their shape but collapse, and the QDs are still in the capsules.

were observed. The size distributions also reflected the formations of Lf-coated rGO or PGP capsules. As shown in Figure 3e and f, the size distributions of PGP capsules ranged from 300 to 380 nm in diameter measured by dynamic light scattering (DLS). Because of the surface charges and polar functional groups of PGP capsules, the hydrodynamic diameters measured by DLS are much larger than that of the dried particles observed under TEM. However, once increasing the rGO concentrations, there was no PGP formation so the measured sizes ranging from 120 to 500 nm (Figure 3g,h) were contributed by random rGO nanosheets and Lf-coated rGO, which is also consistent with the TEM results.

When particles suspensions were irradiated by NIR (808 nm, 2 W cm^{-2}) in PBS, a significant increase in temperature was observed (**Figure 4**a) in the rGO (0.5 mg mL^{-1}) and PGP capsules (5.75 mg mL^{-1}), where PGP capsules contained nearly the same as rGO content according to weight analysis. The temperature rise here was caused by particles absorption, since particle-free PBS solution experienced no NIR-induced heating. In comparison with the solution of rGO, an excellent photon receptor, the PGP capsules solution at the identical rGO concentration displayed a slower rate of temperature rise and a lower final temperature. The different results cannot be explained by the different thermal conductivity (e.g., Lf is a poorer thermal conductor than rGO) because the thermal conductivity only affects the transient rather than the final temperature, which is dominated by photo-absorbance. Such photothermal transition is lower in PGP capsules presumably because the LF coated on rGO surfaces affects photo-absorbance through reflection or deflection. Despite the effect, the PGP capsules still achieved more than 85% of the absorption of pure rGO, which is a strong NIR absorber. In Figure 4b, the loading capacity of a

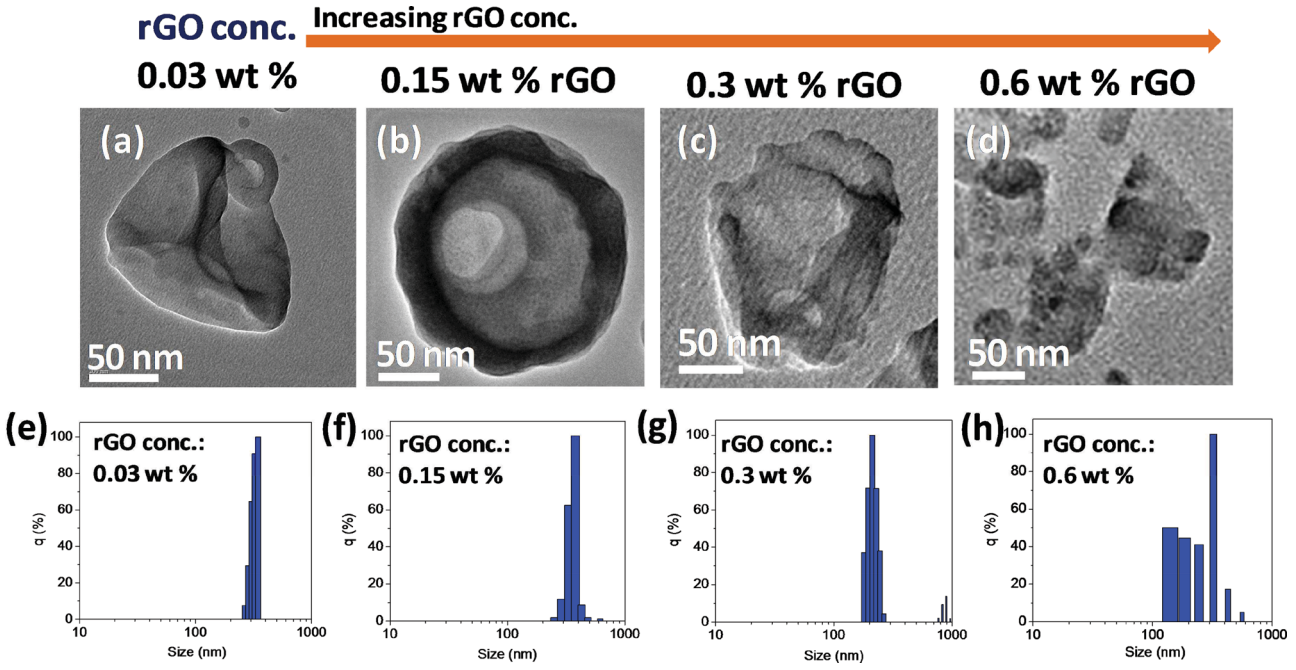

Figure 3. TEM imaging and size distributions of resulting PGP capsules prepared by various rGO concentrations: a,e) 0.03%, b,f) 0.15%, c,g) 0.3%, and d,h) 0.6%.

hydrophilic drug Dox is higher for PGP capsules (9.43 μmol g^{-1} or 5.12 wt%) than for rGO (1.35 μmol g^{-1} or 0.7 wt%) and Lf-coated on rGO (Lf@rGO, 3.81 μmol g^{-1} or 2.07 wt%). This difference cannot be due to the Lf or rGO absorbing alone. Instead, it most likely reflects that the double emulsion process encapsulated the drug molecules in the cores of PGP capsules which offered large space to stabilize the water-soluble Dox as well as prevent them from escaping. Moreover, the watery core of PGP capsules provide not only high loading capacity but also potent encapsulating efficiency (EE%) calculated using formula: EE% = $(W_t/W_i) \times 100\%$, where W_t is the total amount of drug in the capsule suspension and W_i is the total quantity of drug added initially during preparation. Using the double emulsion process to incorporate the hydrophilic drug, the EE% of PGP capsules achieved more than 80%. Oppositely, rGO or Lf@rGO carried drugs only by absorption so the EE% is only about 35% to 46%, respectively. The improvement is related to the two-step emulsifying process. The drug molecules are not only captured in the watery core of PGP capsules during the whole process; some Dox moleucles were also adsorbed on Lf and rGO surfaces because the negative charges of Lf/rGO in the PGP capsule shell provided Coulombic attraction to the positively charged Dox. The behaviors were also evidenced by the drug loading capacity of Lf@rGO composites, which can carry 3.81 μmol Dox per g through adsorption alone (about 40% of PGP capsules).

2.3. Natural and On-demand Drug Release of PGP Capsules

The PGP capsules displayed low natural drug release behavior because the Lf/rGO shells restricted outward Dox diffusion. This scenario is exhibited by the release pattern of Dox without laser treatment in Figure 4c. After 10 h, the Dox only release less than 6% in PBS. Furthermore, to estimate the release behaviors in the intraendo-lysosome environments, the Dox release under pH 5.5 was investigated. The accumulative release of Dox was about 16% and slightly higher than that in PBS due to the acidic environment decreasing the negtive charges of Lf/rGO shells, leading to increased Dox release. However, while applying NIR irradiation for various times, the cumulative release of Dox can be regulated: the longer the NIR treatment, the more drugs released. The released drug from PGP capsules is indicative of a mixture of mechanical actions imposed by the PGP capsules, which may include an "open" configuration of the composite shell and an elastic deformation of capsules, while subjecting instantly to NIR stimulus (SEM image shown in Figure S4, see the Supporting Informaiton). However, some Dox still resided in the capsules because the negatively charged Lf/rGO in the PGP capsule shell provided coulombic attraction to the positively charged Dox. Since NIR is known to cause local heating through the photothermal conversion of rGO, the induced heat would deform the structure or molecular configuration of the Lf-rGO shell. Here, Lf is considered as a thermosensitive polymer because the intermolecular interactions such as hydrogen bonds between peptides will be destroyed (protein unfolding) when the local temperature rises (Figure S5, see the Supporting Information). Therefore, after long-term treatment (10 min), the unrecoverable deformation still maintained a faster sustained release after removing NIR treatment. However, in Figure 4d, when we used shorter NIR-triggered time (1 min), the drug release of PGP capsules follows a burst-to-zero-to-burst staircase-shaped profile, and the release dosage depends on the NIR strength, suggesting the thermally-induced release is an on-demand yet stoppable process. Similarly, the local heating makes the protein unfolding

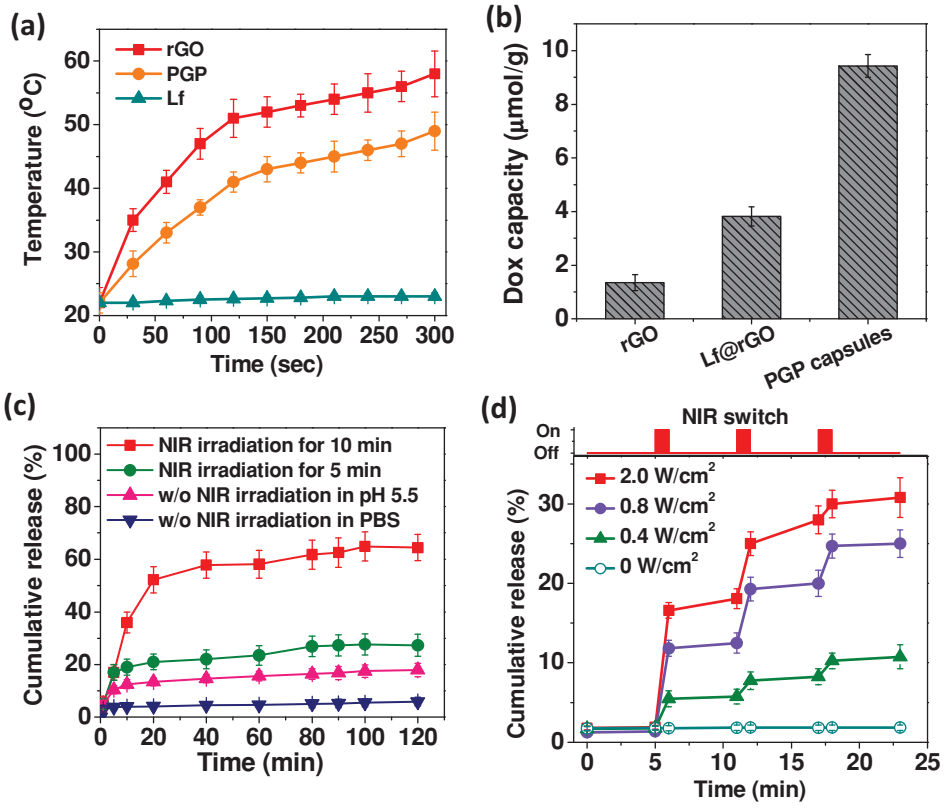

Figure 4. NIR irradiation and drug loading capacity of PGP capsules. a) Heat-generation kinetics of PBS suspension of rGO, PGP capsules and lactoferrin (Lf) under NIR (808 nm, 2 W cm^{-2}) exposure. b) Dox loading in rGO, lactoferrin coating rGO (Lf@rGO), and PGP capsules. c) Natural and NIR-triggered drug release profiles from PGP capsules for 0, 5, and 10 min. d) NIR-triggered drug release from PGP capsules. During the short experiment period, drug release is negligible without NIR triggering. The release rate can be obviously increased while applying NIR irradiation. When the pulsed NIR is set to 0.4, 0.8 and 2 W cm^{-2}, the capsules release drug in a burst–zero–burst fashion.

temporarily but not severely destroyed, enhancing the permeability of the Lf-rGO shells and the drug diffusion rate. Removing the NIR makes the PGP capsules return to their original states, resulting in negligible drug release in short time (e.g., 5 min between treatments). Such protein recovery process can also be understood by peptide thermosensitive behavior: the conformation of some peptides is like a free coil molecule in the warm water due to the weak hydrogen bond interactions but turns into a gel structure which is involved with a triple-helix sequence on cooling.[33,34] Once the temperature rises to about 43 °C, most hydrogen bonds between peptides disappear, possibly loosening the protein–protein interactions and protein intramolecular structures. However, for short-time heating, without dramatically damaging the protein structures, the hydrogen bonds could be recovered after temperature decreased. The SEM images of each sample corresponding to Figure 4c and d after various treatments are also provided in Figure S6 (see the Supporting Information). Besides, similar reversible drug release triggered by thermal heating has also been studied in capsule structures made of polyelectrolytes as well as thermoresponsive hydrogels.[35,36] Therefore, by encapsulating the drug molecules in the thermosensitive Lf-rGO composites, we were able to prevent the drug release naturally as well as manipulate drug release behaviors precisely through tuning NIR strengths and treating time. Moreover, the spectroscopic and cell viability data are also provided to demonstrate that the drug still possesses activity after NIR treatment (Figure S7 in the Supporting Information).

2.4. Cytotoxicity and Cell Uptake of PGP Capsules

Cell viability after PGP capsules treatment was studied using RG2 (a brain cancer cell line as a model cell) and MRC-5 (a human lung fibroblast, normal cell) cells incubated with various PGP capsules. At a dosage of up to 4 mg mL^{-1} PGP capsules for 24 h we demonstrated that the drug-free capsules showed no toxic (cell viability about 93% ± 6%) to cells (**Figure 5**). Next, to evaluate the targeting specificity of the PGP capsules, the RG2 cells with high expression level of Lf receptors were incubated with the capsules.[37,38] For comparison, MRC-5 cells with relatively low level of Lf receptors were used. We have confirmed the Lf expression of two cell lines by labeling cell with fluorescently-labeled Lf. Flow cytometry measurements showed that the fluorescence of stained RG2 cells is 10–20 times higher than that of MRC-5 cells (data not shown). After 4 h incubation with PGP capsules, highly fluorescent PGP capsules (labeled by Cy5.5) are observed with confocal fluorescence imaging and most PGP capsules surround the nuclei, suggesting the high targeting efficacy and internalized ability (**Figure 6**a to d). The cross-sectional confocal image in Figure 6e for RG2 cells incubated with PGP capsules also verified that many regions of the cytoplasm contain these nanoparticles, a further confirmation of their effective internalization. To understand the targeting effect of Lf, the amphiphilic PVA (poly(vinyl alcohol)) as model polymer surfactant was applied to fabricate the PVA-GO capsules in the control experiment (here, we chose PVA because it possesses no any targeting functions and neutral properties). The flow cytometry analysis in Figure 6f significantly shows that the fluorescence intensity (the horizontal axis) of PGP capsules (labelled by QDs) in RG2 cells was approximately 10 times than that of PVA-GO capsules. The results reveal that the PGP capsules possessing the Lf surface provide a greater internalized efficiency than other capsules without the functional surface. In contrast, compared to RG2, both fluorescence intensities of PGP and PVA-GO capsules in MCR-5 cells are relatively low under identical incubation time, indicating no

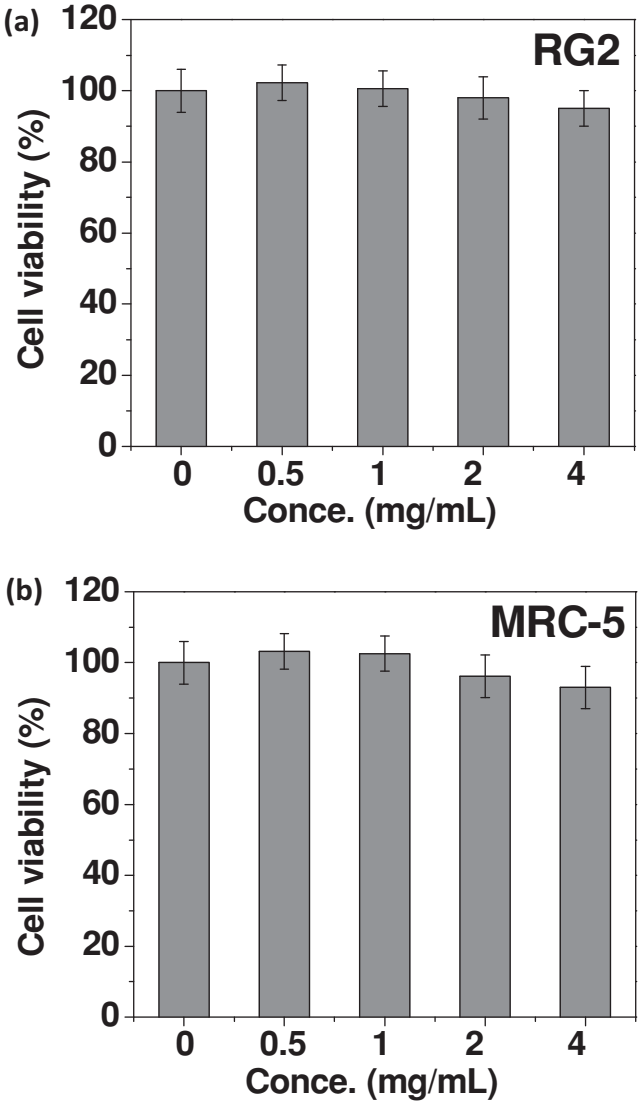

Figure 5. Cell viability of: a) RG2, and, b) MRc-5 cells after 24 h incubation with various concentrations of PGP capsules. Cell viability was measured using the trypan blue counting method.

strong interaction between cell surface and particles (Figure S8, see the Supporting Information). The fluorescence intensity of PGP is twice than that of PVA-GO capsules for MCR-5 cells, which was possibly caused by different surface properties.

2.5. Photochemothermal Therapy of PGP Capsules

To estimate the photochemothermal therapy of PGP capsules, an in vitro study was conducted on RG2 cells incubated with PGP capsules loaded with 0.05 and 0.25 μg mL^{-1} of Dox (termed as PGP-Dox(0.05) and PGP-Dox(0.25), respectively). After incubated with i) no particle (control), ii) Dox-free PGP capsules, iii) PGP-Dox(0.05), and iv) PGP-Dox(0.25) for 1 h, the cells were exposed to NIR irradiation (2 W cm^{-2}) for 5 min. Then, the cells were stained with two fluorescence dyes to characterize cell viability: live cells appeared green, dead cells appeared red (**Figure 7**a to d). The result shows no cell kill by NIR alone (Control, Figure 7a), but most kill appear at the irradiated area (the red fluorescence dead cells, Figure 7b) by the combined effect of NIR laser irradiation and PGP capsules. However, in the area out of irradiation, most cancer cells still survived (the green fluorescence live cells). Because the NIR laser irradiation is a focal light which can directly increase the temperature of PGP capsule through photothermal conversion, the local heat induced by NIR irradiation is only strong enough to kill the cells irradiated by light. However, out of NIR irradiation, such local heat cannot obviously influence the surrounding cell's viability even through the temperature of cell medium increased about 3 °C. In contrast, once the PGP-Dox(0.25) were combined with photothermal therapy, not only the cells within the area of irradiation but also those surrounding ones were killed (Figure 7c). Compared to Dox only, 0.25 μg mL^{-1} of Dox can cause 50% cell apoptosis (i.e., the half maximal inhibitory concentration (IC_{50}) of Dox is 0.25 μg mL^{-1}). Importantly, when the drug concentration loaded into the PGP capsules was 5 times lower (PGP-Dox(0.05)) than the IC_{50} of Dox, the photochemothermal therapy can still kill more than 95% of cancer cells. Quantification of cell viability under various treatments is provided in Figure 7e. Despite the photothermal cell killing effect being strong in the center of the cell dish, without the assistance of Dox the cell viability of RG2 treated by PGP+NIR reached more than 80%, indicating that NIR only damages the small area of cells exposed to light. However, the clear influences on cell killing can be observed on loading Dox in PGP capsules. When RG2 cell treated by PGP-Dox(0.25), applying 5 min NIR irradiation can cause 94% cell death, which is much higher than Dox (50% cell death) or PGP along. Furthermore, at only 1/5 of the drug dosage (PGP-Dox(0.05)), the photochemotherapy of PGP capsules can still kill cells over a larger region, and the cell viability decreases to 10%. The strong synergistically thermo- and chemo- effect for cell killing can be observed clearly. The results demonstrated two important factors on photo-chemo-thermal therapy: i) photochemothermal therapy induced by PGP capsules killed not only the cells exposed by light but also the cells surrounded the photo-treating area; and, ii) applying NIR irradiation not only leads to free Dox release from PGP capsules but also enhances the Dox therapeutic efficiency.

The improvements inducing a wider range of cell therapeutic effect than just the irradiation area can be understood by several mechanisms. i) Thermal sensitive structures of PGP capsules with low transition temperatures, so the local photothermal heating significantly causes the PGP capsules to release Dox. ii) Furthermore, the Lf targeting ability of PGP capsules also improved cell uptakes, enhancing the Dox release in the targeted cells. iii) The interaction of heat and chemotherapeutic agents impreoved cellular drug uptake, DNA damage, and inhibition of DNA repair.[39,40] Therefore, in this work, integrating the high cell uptake and thermochemotherapy, the drugs can be precisely delivered into cells and released on-demand in the cells, revealing the great potentiation of excellent therapeutic efficacy even with low drug dosage. Such modality for cancer therapy not only mitigates the side effect but also provides great potential to eradicate the malignant cells which are out of irradiated treatment.

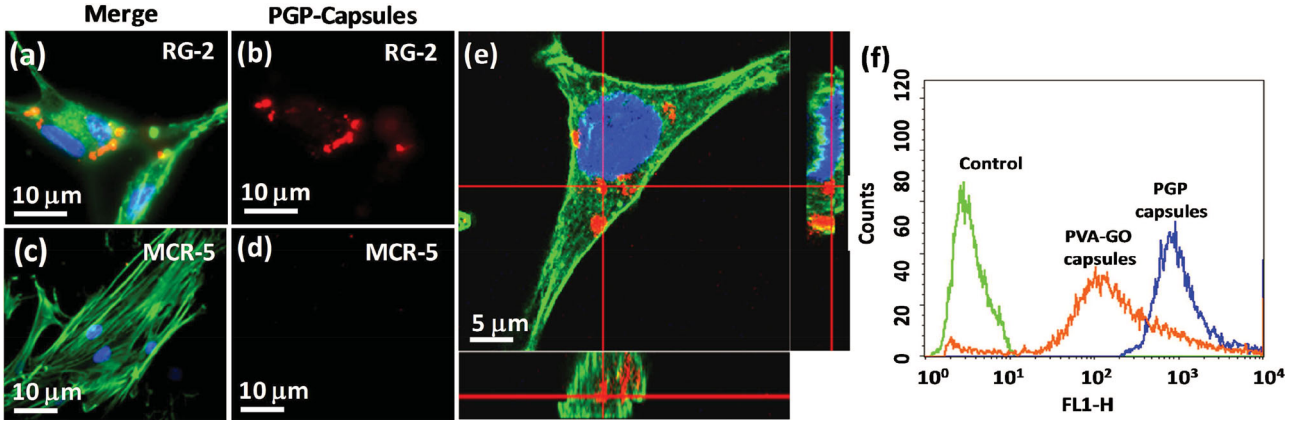

Figure 6. Cellular uptake of PGP capsules in: a,b) RG-2 cells showing cy5.5-labeled PGP capsules fluorescence (red) in many regions including blue ones (cytoplasm), and. c,d) MCR-5 cells showing rare cy5.5-labeled PGP capsules at cell surfaces. e) Confocal images of multiple cross-sections exhibiting various locations of PGP capsules within cells. f) Flow cytometry histograms of RG2 cells after incubation with PGP capsules and PVA-GO capsules.

2.6. In Vivo Photochemothermal Therapy

In vivo targeting efficacy was conducted in nude mice bearing RG2 tumor cells. We injected 100 μL solution which contained 0.5 wt% PGP capsules labeled by Cy5.5 via the tail vein of nude mice. The fluorescence signals from Cy5.5 (Cy5.5 channel, Ex: 640 nm, Em: 710 nm) was found after both 1 and 5 d, and the intensity showed no significant decrease, indicating the successful targeting and internalizing of PGP capsules to the tumor cells (**Figure 8**a). The targeting efficacy are mainly contributed by the Lf on PGP capsules which can rapidly attach on the RG2 cells and enhance the uptake efficiency.[41] Next, we investigated the biodistribution of the PGP capsules as shown in Figure S9 (see the Supporting Information). Consistent with the in vitro results, we found that targeted-PGP capsules also improved the accumulation in tumors in vivo. We intravenously (i.v.) injected PGP capsules-Cy5.5 and non-targeted (PVA-rGO capsules)-Cy5.5 through tail veins into nude mice bearing RG2 tumors. Major organs in addition to tumors were excised at 24 and 48 h after injection to assess the biodistribution of capsules using an IVIS spectral imaging system (LifeScience, USA). As shown in Figure S9a, PGP capsules are more efficiently accumulated in the tumor than non-targeted capsules. Although the latter showed some weak accumulation in the tumor 24 h post-injection, presumably because of the enhanced permeability and retention (EPR) effects, the fluorescence signal was washed out after 48 h, indicating poor binding ability of non-targeted capsules to cells. In contrast, PGP capsules displayed strong accumulation in the tumor at both 24 and 48 h, indicating that the cell targeting of the PGP capsules can improve in persistent internalization. Furthermore, to investigate the biodistribution of PGP capsules, following the reports,[42,43] we injected 100 μL solution, which contained 0.5 wt% PGP capsules labeled by CdSe quantum dots, via the tail vein of nude mice. Quantitative measurements of Cd amount of the PGP capsules in each organ by ICP-MS are displayed in Figure S9b. Furthermore, at 24 h post-injection, the amount of PGP capsules was about 86.6 μg in the 105 mg tumor, which was estimated from the biodistribution results. Then, the mouse was next exposed to a NIR irradiation (2 W cm^{-2}) for 3 min during which the temperature in the tumor increased from 31 to 55 °C (Figure 8b). For control, mouse injected with saline or Dox alone was also irradiated but displayed no temperature increase. In Figure 8c, to compare that the PGP-Dox-NIR treatment is superior to chemotherapy or NIR treatment alone, and that PGP capsule is essential for achieving superiority, tumor bearing mice were investigated to receive the following treatments, PBS+NIR (control), Dox+NIR (combine treatment without PGP capsules), PGP+NIR, and PGP-Dox+NIR. (intravenous injection was applied and the power density of NIR irradiation was 2 W cm^{-2}.) Only PGP-Dox+NIR resulted in a reduction of the tumor size although PGP+NIR arrested tumor growth for the first 5 d. These results confirmed the therapeutic effects of the NIR irradiation (i.e., photothermal therapy), mediated here by rGO in PGP capsules, as evidenced by the drug-free treatment (PGP+NIR) and free drug (Dox+NIR treatment), but it is the combined use of NIR irradiation and drug encapsulated in PGP that is most effective. Although this NIR irradiated system still exists barrier to be directly applied for brain tumor due to the technical issue, the laser interstitial thermal therapy fabricated by Monteris Medical, Inc. has been used for conformal laser thermal coagulation of deep-seated brain tumors using a side-firing laser probe in clinical trials.[44] Such techniques may offer the great potential to combine the laser treatment and drug-delivery system.

At a closer observation, the tumor recurrence after PGP+NIR treatment occurred in the area surrounding the NIR treated area (Figure 8d). The cancer cells as a scab in the center of tumor did not re-grow, but the cell dodging the NIR treatment developed to form the new solid tumor after 14 d. The results suggest that when only applying the NIR treatment to a local cancer therapy, it is difficult to eradicate all cancer cells at once and the survival cells proliferate continuously to form a new tumor again. However, combining the photothermal with chemotherapy, the PGP-Dox+NIR apparently showed no tumor recurrence after 2 months, indicating that the anticancer drug release not only affected the treating area locally but also killed closeby cells. Actually, the temperature of whole

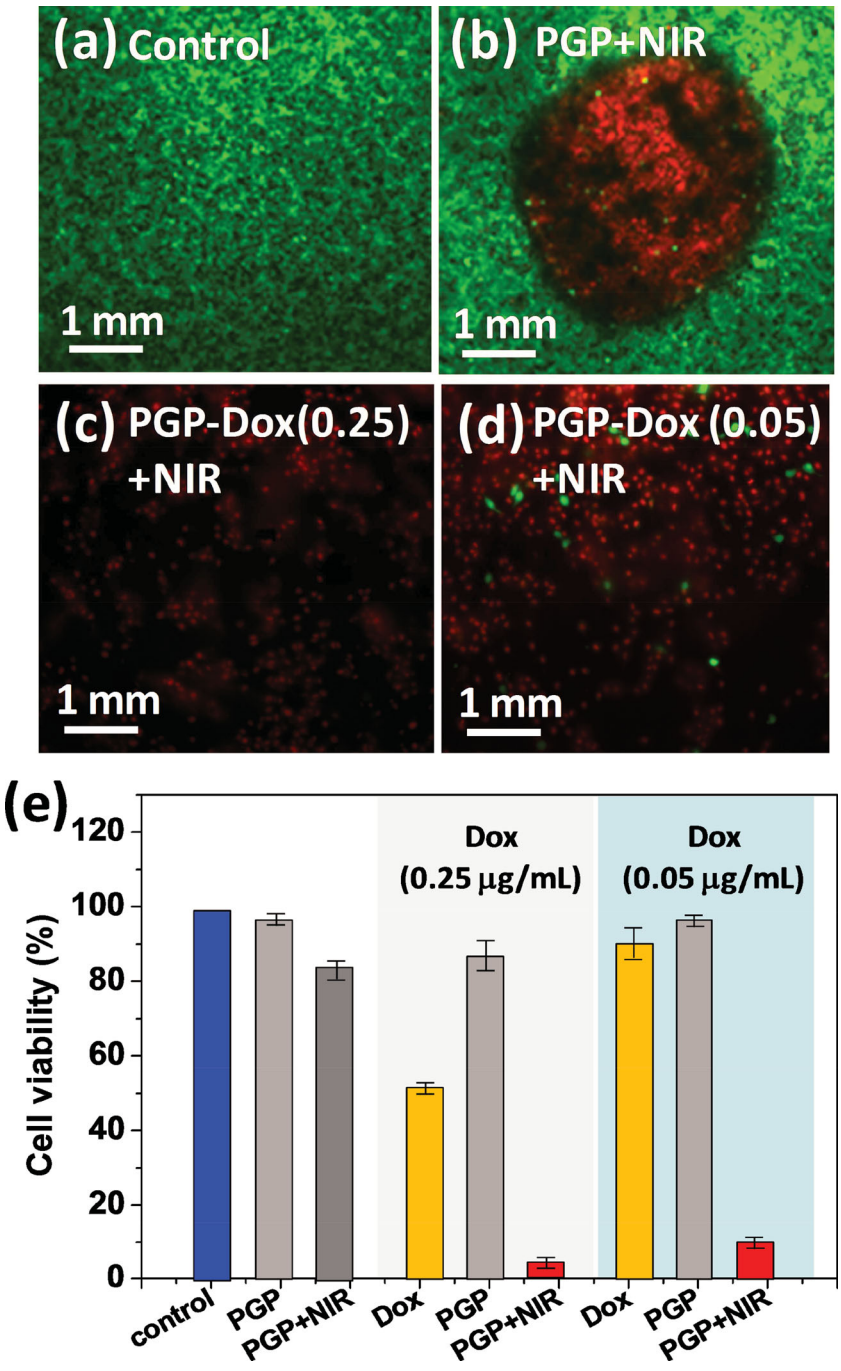

Figure 7. NIR-induced in vitro photothermochemo thrapy. Fluorescent images of RG-2 cells: cells incubated without PGP capsules as: a) control, compared with cells incubated with: b) PGP capsules, c) PGP-Dox(0.25), and d) PGP-Dox(0.05) under NIR treatment; green fluorescent cells are live and red fluorescent cells are dead. e) Cell viability after incubating RG2 cells for 24 h with PGP capsules of following types: control (without PGP capsules), PGP capsules, PGP capsules with NIR treatment for 5 min, and PGP containing different Dox concentrations with NIR treatment for 5 min.

tumor can reach about 50 °C even when the area is not at the NIR laser point, which may also promote drug release and penetration since the PGP capsules are highly thermally sensitive. Meanwhile, judging from the absence of weight loss shown in Figure 8e, there appears to be little side effect/systemic toxicity of either thermal- or thermal-chemotherapy when administered with our engineered PGP capsules system, with or without drugs.

Lastly, tissues of the same mice receiving intravenous injection of PGP capsules and NIR treatment were histologically investigated. Hematoxylin and eosin (H&E)-stained tissue slices from major clearance organs (heart, lung, liver, spleen, and kidney) obtained 7 d post treatment showed no significant sign of damage (Figure S10a, see the Supporting Information), implying no severe toxicity of the PGP-Dox+NIR treatment to non-tumor sites. In contrast, in tumor slices taken from both PGP+NIR and PGP-Dox+NIR treated mice, large areas of dead cells without nuclei were found (Figure S10b). Meanwhile, under other treatments not involving PGP, Dox, or NIR, many nuclei still existed in the tumor slices. A further comparison of the large nuclei-free area (indicating tumor cell kill) and nucleus apoptosis confirmed that the synergistic thermal and chemotherapeutic effects (PGP-Dox+NIR) are more effective than thermal effect alone (PGP+NIR) and chemotherapy alone (PGP-Dox). Therefore, direct histological evidence has corroborated our tumor size measurements in vivo (Figure 8c) and cell viability data in vitro (Figure 7e,f) concerning the efficacy of PGP-Dox+NIR treatment. It has also confirmed our biodistribution observations that PGP-based drugs seem to have mostly benign side effects on non-tumor sites.

3. Conclusion

In summary, i) we have developed a simple, versatile and scalable method to fabricate core–shell capsules with a single-component-protein lactoferrin shell stabilized by reduced graphene oxide nanosheets. The capsules were capable of encapsulating hydrophilic Dox with high efficiency. ii) On-demand drug release in vitro and in vivo can be achieved by applying NIR irradiation. The release patterns exhibit features of fast on/off-acting and precise strength-dosage dependence, making it highly controllable. iii) In vitro cell kill and in vivo tumor growth suppression not only in the phototreating area but also widely surrounding tumor cells by thermal-chemotherapy have been demonstrated using drug-containing PGP capsules, with little side effect. iv) We suggest the delivery system developed here can facilitate various theranostic applications that combine

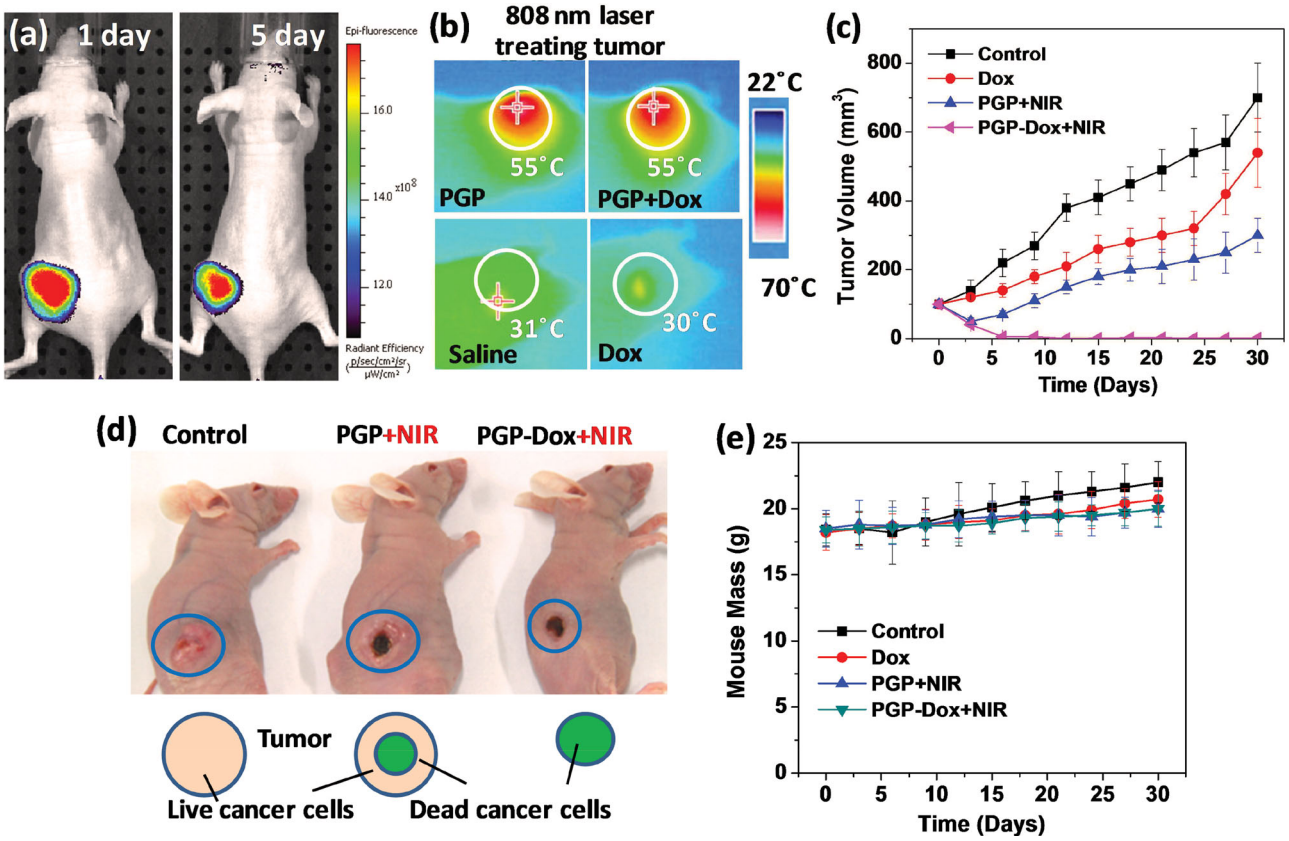

Figure 8. In vivo study of PGP capsules. a) Fluorescence images of RG2 tumor bearing mice 1 and 5 d after PGP capsules injection (i.v.). b) Infrared thermal images of RG2 tumor-bearing nude mouse under PGP+NIR treatment. c) Tumor therapy using PGP capsules with/without drugs and with/without NIR treatment for 5 min at 24 h post-injection. d) RG2 tumor treated by PGP+NIR (middle) and PGP-Dox+NIR (right) after 2 months. The results indicate that NIR alone treatment did not eradicate all cancer cells at once and the survival cells proliferate continuously to form the new tumor again. However, combining the photothermal and chemotherapy, the tumor recurrence can be avoided. e) Mouse mass as a function of days post-treatment displaying no loss for 30 d in all groups.

high dosage drugs, target/remote-field sensing, on-demand drug release, hyperthermia, and bio-imaging. Such functional drug delivery system may offer a new avenue for cancer therapy and other clinical applications.

4. Experimental Section

Synthesis of Small-sized rGO: The reduced graphene oxide nanosheets (rGO) was prepared by a modified Hammer method.[45] Briefly, native graphite flakes were preoxidized by mixing with H_2SO_4, $K_2S_2O_8$, and P_2O_5 and heated at 80 °C for 12 h. Then, washing with distilled water and ethanol, the flakes were dried overnight in an oven under nitrogen. Subsequently, the preoxidized graphite powder was oxidized by using in H_2SO_4 at 0 °C, and then adding $KMnO_4$ slowly with stirring. The mixture was continuously stirred in an ice bath for 2 h before the reaction was terminated with distilled water. To remove MnO_2, H_2O_2 was added until the mixture color changed to bright yellow. The purification of the graphite oxide powder was carried out by adding 1% HCl and centrifuging at 6000 rpm for 10 min, followed by washing 3 times with an excess of distilled water until reaching pH 6–7. Then, the precipitate was redispersed in distilled water. An ultrasonic probe was used to exfoliate the oxidized graphite, and the resulting small-size GO was collected from the supernatant by centrifugation at 12 000 rpm for 30 min. The supernatant (GO content: 3 mg mL^{-1}, pH 6–7) did not precipitate over several months. To form rGO, the dispersion of GO was added to dilute ammonia solution to adjust the solution to pH 11.5–11.8, and then, the solution was heated to 80 °C for 12 h. After reduction of the GO (the color of the solution turned from brown to black), the rGO aggregates were sonicated for 1 h to exfoliate the rGO sheet stacks to become a stable colloidal solution. Then, the dispersion was centrifugated at 12 000 rpm for 30 min to remove the precipitates of large-size rGO sheets. Finally, the small-size rGO sheets were in the supernatant (rGO content: 1.2–1.5 mg mL^{-1}, pH 11.3–11.4).

Measurement of Hydrophilic-Lipophilic Balance (HLB) Value of Lactoferrin (Lf): First, Span 80 (HLB = 4.3) and Tween 80 (HLB = 15) were mixed to prepare reference oils of different HLB values from 4 to 15 using the formulus, HLB = $\%HLB_{Span} + \%HLB_{Tween}$.[46] Then, 1.5 mL reference oil was added to 8 mL water and 0.5 mL Lf to form an emulsion (here, Lf is regarded as a surfactant). The surfactant is deemed to have the same HLB value as the reference oil if and only if it enables a stable emulsion to be maintained for 24 h after initial sonification. In this way, the HLB of Lf was determined as shown in Figure S1 (see the Supporting Information).

Synthesis of Core–Shell Protein–Graphene–Protein (PGP) Capsules: Firstly, the superhydrophobic rGO was synthesized following Lin et al.[22] with a mixture of 100 mg of rGO and 400 mg of octadeylamine amine (ODA) in 100 mL ethanol solution for 2 h at room temperature. Then, the rGO was separated by filtration using a nylon membrane (pore size is 0.2 μm) and washed by ethanol for several times to remove the excess aliphatic amine. Finally, the rGO can be re-dispersed in chloroform.

To synthesize rGO-containing capsules (PGP capsules) and encapsulating doxorubicin (Dox), a two-step double emulsion process was employed. We dispersed 0.75 mg of hydrophobic rGO in 250 mL chloroform as an oil phase, and dissolved 2 mg of Lf and 0.5 mg of Dox in the 100 µL of de-ionized water (DI water) to form a water phase. Then the water phase was added to the oil phase, and the mixture was emulsified by ultrasonification (20 kHz, 130 W) for 1 min to form W/O emulsion. The second step of W/O/W emulsion was subsequently carried out by adding the W/O emulsion to 400 µL of 2% Lf, and the mixture was emulsified again by similar approach before stirring at room temperature to completely evaporate the organic solvent. The product was purified and washed by DI-water to remove free Dox and proteins by centrifugation at 6000 rpm, and the purification step was repeated 2 times. Since water-soluble quantum dots (QDs, Oceantech, USA) have the same hydrophilic property as Dox, they were incorporated into PGP capsules at the same time as was Dox.

Characterization: The UV-Vis spectra of PGP capsules were investigated by Hitachi U-2900 UV-Vis Double Beam Spectrophotometer. The morphologies of PGP capsules were analyzed by a field-emission scanning electron microscope (FE-SEM, JEOL-6500, Japan) and a transmission electron microscope (TEM, JEM-2100, Japan). For SEM analysis, PGP capsules was dried on a silicon wafer and coated via sputtering with platinum. Dynamic light scattering (DLS, BECKMAN COULTER Delsa Nano C particle analyzer) was used to determine the sizes of particles.

Drug Loading and In Vitro Drug Release: Two-step emulsification as describe above was used to achieve high encapsulation efficiency of Dox (initial Dox concentration: 0.5 mg per 100 µL de-ionized water (DI-water) in the first emulsion step). The drug loading capacity of PGP capsules was calsulated by the following equation: %Loading capacity = Amount of drug loaded × 100/Amount of PGP capsules. The encapsulation efficiency (EE%) of Dox was calculated according to the equation: Encapsulation efficiency (EE%) = (W_t / W_i) × 100%, where W_t is the total amount of drug in the capsule suspension and W_i is the total quantity of drug added initially during preparation. Dox was quantified by UV-Vis spectrometer (Evolution 300, Thermo) at a wavelength of 488 nm, a characteristic absorption band of Dox. For drug release test, Dox-containing capsules were suspended in phosphate buffered saline (PBS) solution. Prior to the test, the nanocapsules were first washed by PBS (pH 7.4), followed by washing with DI water. At various time points during release, some PBS sample was taken and centrifuged at 5000 rpm to separate PBS from nanocapsules, and the supernatant was analyzed by UV-Vis to examine the Dox concentration due to release.

Near-Infrared (NIR)-Triggered Release: Near-infrared (NIR) was used to activate/heat the PGP capsules. Suspension of Dox-loaded PGP capsules was placed into tubes and treated by NIR of different magnitude (0.4, 0.8, and 2.0 W cm^{-2}). After the treatment, an infrared thermometer was used to measure the temperature and drug release patterns were determined by UV-Vis spectroscopy.

Cytotoxicity of PGP Capsules: RG2 (a brain cancer cell line) and MRC-5 (a human lung fibroblast, normal cell) cells were cultured in Eagle's minimum essential medium, supplemented with 10% fetal bovine serum and 1% penicillin/streptomycin, at 37 °C in a 5% CO_2-enriched atmosphere. 0.5 to 2 mg mL^{-1} of PGP capsules were incubated with cancer cells for 24 h and its effects on cell viability was evaluated by a counting method based on trypan blue exclusion. After being removed from dishes by trypsin, cells were collected and diluted (1:4) with trypan blue and scored under light microscopy. The surviving cells (unstained) were manually counted up to 3 times per application and at least 3 individual experiments were undertaken per treatment group. The results were expressed as percentage of viable cells.

Cellular Uptake of PGP Capsules: To facilitate observing cellular uptake, the fluorescent dye, 25 mM of Cy5.5-NHS (Lumiprobe corporation, USA), was conjugated to the PGP capsules via *N*-(3-dimethylaminopropyl)-*N′*-ethylcarbodiimide (EDC) coupling method overnight at room temperature (the molar ratio of Cy5.5-NHS/Lf was 1:1.). After reaction, un-reacted Cy5.5 and EDC molecules were removed by centrifuging at 6000 rpm for 10 min and washed 3 times with PBS solution (pH = 7.4). Cellular uptake of PGP capsules was studied by fluorescence and confocal microscope. Cells were seeded and grown on glass coverslips for 24 h and then treated with nanocapsules for various time. After washing in PBS and fixed for 30 min with 3% formaldehyde, permeabilization was performed with 0.1% Triton X-100 (J.T. Beker) in PBS for another 30 min. Cells were subsequently washed two more times in PBS and stained with DAPI (1 µg mL^{-1}) for 30 min and with f-actin (300 units per mL; Alexa Fluor 488 phalloidin) solution for another 30 min. Finally, they were mounted (using Dako mounting solution) on fresh glass slides and observed under fluorescence or confocal microscopy.

In Vitro Live/Dead Cell Imaging after NIR irradiation: RG2 cells grown in 24-well cell culture plates for 24 h were incubated for 4 h with PGP capsules with or without loading Dox. Subsequently, the RG2 cells mixed with PGP capsules were washed two times with PBS solution to remove the excess capsules. Then, the plate was exposured to NIR light (808 nm, 2 W cm^{-2}) for 0 or 5 min. Following irradiation, the cells were stained using a LIVE/DEAD cell viability assays (Life Technology, USA).

In Vivo Fluorescence Imaging and Photochemothermal Therapy: All animals were obtained from BioLASCO Taiwan Co. (Taiwan) and handled in accordance with the guidelines for Animal Care and Use Committee of the Institute of Life Science of National Chiao Tung University. To induce solid tumors, RG2 cells (1×10^5 in 100 mL PBS) were injected into female nude mice (CAnN.Cg-Foxn) of 6 to 7 weeks old. When the tumor grew to approximately 5 mm in diameter, the nude mice were ready for biodistribution and therapeutic studies. For in vivo fluorescence purpose, the fluorescent dye, 25 mM of Cy5.5-NHS, was conjugated to the PGP capsules via *N*-(3-dimethylaminopropyl)-*N′*-ethylcarbodiimide (EDC) coupling method overnight at room temperature (the molar ratio of Cy5.5-NHS/Lf was 1:1.). After reaction, unreacted Cy5.5 and EDC molecules were removed by centrifuging at 6000 rpm for 10 min and washing 3 times with PBS solution (pH = 7.4). Then, 100 µL saline solution containing 0.5 wt% of PGP-Cy5.5 was i.v. injected into the mice through the tail vein (the total injection amount of PGP-Dox capsules is 25 mg per kg nude mice and the amount of Dox is 1.28 mg per kg nude mice.). Fluorescent images were investigated by IVIS Spectrum (IVIS imaging System 200 Series, Caliper Life Science, USA). Living Image software Version 3.0 (Xenogen) was used to acquire and quantify the fluorescence 1 and 5 d after injection (Cy5.5 channel, ex = 640 nm, em = 710 nm). In vivo combined photochemothermal therapy was carried out by an optical-fiber-coupled 808 nm highpower laser diode at a power density of 2 W cm^{-2} for 5 min to irradiate tumor 1 d after injection. To avoid excessive heat damage, NIR irradiation was administered intermittently as follows: 60 s on/10 s off, repeated five times. The tumor sizes were measured with a caliper and volumes were calculated as (tumor length) × (tumor width)^2/2. The relative tumor volumes were calculated as V/V_0 (where V_0 was the tumor volume when the treatment was initiated). All measurements were performed in triplicate.

Supporting Information

Supporting Information is available from the Wiley Online Library or from the author.

Acknowledgements

This work was financially supported by the National Science Council of the Republic of China, Taiwan under contracts NSC 102-2221-E-009 -023 -MY3 and NSC 102-2218-E-007-014 and by the "Aim for the Top University" program of the National Chiao Tung University and the Ministry of Education, Taiwan, R.O.C. I.-W.C. acknowledges support from Army Medical Research & Material Command Grant No. W81XWH-10-1-0320 and W81XWH-10-1-0604.

Received: January 9, 2014
Revised: February 7, 2014
Published online: April 2, 2014

[1] A. F. Bagley, S. Hill, G. S. Rogers, S. N. Bhatia, *ACS Nano* **2013**, *7*, 8089.
[2] H. Kim, D. Lee, J. Kim, T. I. Kim, W. J. Kim, *ACS Nano* **2013**, *7*, 6735.
[3] C. C. Huang, C. H. Su, W. M. Li, T. Y. Liu, J. H. Chen, C. S. Yeh, *Adv. Funct. Mater.* **2009**, *19*, 249.
[4] K. Yang, L. Feng, X. Shi, Z. Liu, *Chem. Soc. Rev.* **2013**, *42*, 530.
[5] B. Tian, C. Wang, S. Zhang, L. Feng, Z. Liu, *ACS Nano* **2011**, *5*, 7000.
[6] K. Yang, S. Zhang, G. Zhang, X. Sun, S. T. Lee, Z. Liu, *Nano Lett.* **2010**, *10*, 3318.
[7] T. M. Allen, P. R. Cullis, *Science* **2004**, *303*, 1818.
[8] D. Peer, J. M. Karp, S. Hong, O. C. Farokhzad, R. Margalit, R. Langer, *Nat. Nanotechnol.* **2007**, *2*, 751.
[9] Z. Xiao, C. Ji, J. Shi, E. M. Pridgen, J. Frieder, J. Wu, O. C. Farokhzad, *Angew. Chem. Int. Ed.* **2012**, *51*, 11853.
[10] B. M. Chang, H. H. Lin, L. J. Su, W. D. Lin, R. J. Lin, Y. K. Tzeng, R. T. Lee, Y. C. Lee, A. L. Yu, H. C. Chang, *Adv. Funct. Mater.* **2013**, *23*, 5737.
[11] C. E. Ashley, E. C. Carnes, G. K. Phillips, D. Padilla, P. N. Durfee, P. A. Brown, T. N. Hanna, J. Liu, B. Phillips, M. B. Carter, N. J. Carroll, X. Jiang, D. R. Dunphy, C. L. Willman, D. N. Petsev, D. G. Evans, A. N. Parikh, B. Chackerian, W. Wharton, D. S. Peabody, C. J. Brinker, *Nat. Mater.* **2011**, *10*, 389.
[12] B. J. Hong, O. C. Compton, Z. An, I. Eryazici, S. T. Nguyen, *ACS Nano* **2012**, *6*, 63.
[13] M. Cui, D. J. Naczynski, M. Zevon, C. K. Griffith, L. Sheihet, I. Poventud-Fuentes, S. Chen, C. M. Roth, P. V. Moghe, *Adv. Healthcare Mater.* **2013**, *9*, 1236.
[14] S. H. Hu, S. Y. Chen, X. Gao, *ACS Nano* **2012**, *6*, 2558.
[15] S. H. Hu, B. J. Liao, C. S. Chiang, P. J. Chen, I. W. Chen, S. Y. Chen, *Adv. Mater.* **2012**, *24*, 3627.
[16] S. Zhou, J. Fan, S. S. Datta, M. Guo, X. Guo, D. A. Weitz, *Adv. Funct. Mater.* **2013**, *23*, 5925.
[17] M. H. Lee, K. C. Hribar, T. Brugarolas, N. P. Kamat, J. A. Burdick, D. Lee, *Adv. Funct. Mater.* **2012**, *22*, 131.
[18] J. A. Hanson, C. B. Chang, S. M. Graves, Z. Li, T. G. Mason, T. J. Deming, *Nature* **2008**, *455*, 85.
[19] W. Yafei, Z. Tao, H. Gang, *Langmuir* **2006**, *22*, 67.
[20] R. Qiao, Q. Jia, S. Hüwel, R. Xia, T. Liu, F. Gao, H. J. Galla, M. Gao, *ACS Nano* **2012**, *6*, 3304.
[21] Z. Pang, L. Feng, R. Hua, J. Chen, H. Gao, S. Pan, X. Jiang, P. Zhang, *Mol. Pharm.* **2010**, *7*, 1995.
[22] H. Chen, Y. Qin, Q. Zhang, W. Jiang, L. Tang, J. Liu, Q. He, *Eur. J. Pharm. Sci.* **2011**, *44*, 164.
[23] D. A. Bricarello, J. T. Smilowitz, A. M. Zivkovic, J. B. German, A. N. Parikh, *ACS Nano* **2011**, *5*, 42.
[24] Z. Li, M. Xiao, J. Wang, T. Ngai, *Macromol. Rapid Commun.* **2013**, *34*, 169.
[25] Z. Lin, Y. Liu, C. P. Wong, *Langmuir* **2010**, *26*, 16110.
[26] Y. Wang, K. Wang, J. Zhao, X. Liu, J. Bu, X. Yan, R. Huang, *J. Am. Chem. Soc.* **2013**, *135*, 4799.
[27] Y. Liu, X. Dong, P. Chen, *Chem. Soc. Rev.* **2012**, *41*, 2283.
[28] K. Szaciłowski, W. Macyk, A. Drzewiecka-Matuszek, M. Brindell, G. Stochel, *Chem. Rev.* **2005**, *105*, 2647.
[29] S. Mura, J. Nicolas, P. Couvreur, *Nat. Mater.* **2013**, *20*, 991.
[30] S. U. Pickering, *J. Chem. Soc.* **1907**, *19*, 2001.
[31] B. P. Binks, T. S. Horozov, *Colloidal Particles at Liquid Interfaces*, Cambridge University Press, Cambridge **2006**.
[32] C. Miesch, I. Kosif, E. Lee, J. K. Kim, T. P. Russell, R. C. Hayward, T. Emrick, *Angew. Chem. Int. Ed.* **2012**, *51*, 145.
[33] S. H. Hu, T. Y. Liu, D. M. Liu, S. Y. Chen, *Macromolecules* **2007**, *40*, 6786.
[34] V. Crescenzi, A. Francescangeli, A. Taglienti, *Biomacromolecules* **2002**, *3*, 1384.
[35] S. H. Choi, J. H. Lee, S. M. Choi, T. G. Park, *Langmuir* **2006**, *22*, 1758.
[36] A. M. Derfus, G. von Maltzahn, T. J. Harris, T. Duza, K. S. Vecchio, E. Ruoslahti, S. N. Bhatia, *Adv. Mater.* **2007**, *19*, 3932.
[37] E. Van Uden, G. Carlson, P. St. George-Hyslop, D. Westaway, R. Orlando, M. Mallory, E. Rockenstein, E. Masliah, *Mol. Cell Neurosci.* **1999**, *14*, 129.
[38] L. Maletínská, E. A. Blakely, K. A. Bjornstad, D. F. Deen, L. J. Knoff, T. M. Forte, *Cancer Res.* **2000**, *15*, 2300.
[39] M. Urano, M. Kuroda, Y. Nishimura, *Int. J. Hyperthermia* **1999**, *15*, 79.
[40] M. H. Falk, R. D. Issels, *Int. J. Hyperthermia* **2001**, *17*, 1.
[41] R. F. Barth, B. Kaur, *J. Neurooncol.* **2009**, *94*, 299.
[42] J. R. Roberts, J. M. Antonini, D. W. Porter, R. S. Chapman, J. F. Scabilloni, S. H. Young, D. Schwegler-Berry, V. Castranova, R. R. Mercer, *Part Fibre Toxicol.* **2013**, *10*, 5.
[43] L. Ye, K. T. Yong, L. Liu, I. Roy, R. Hu, J. Zhu, H. Cai, W. C. Law, J. Liu, K. Wang, J. Liu, Y. Liu, Y. Hu, X. Zhang, M. T. Swihart, P. N. Prasad, *Nat. Nanotechnol.* **2012**, *7*, 453.
[44] E. S. Andrew, S. A. Manmeet, V. P. Jose, M. Sunil, G. T. Mark, E. J. Stephen, L. S. Jeffrey, P. Michael, A. G. Mark, C. Mark, B. Cathy, J. Jennifer, V. M. Mary, D. Dawn, D. Gail, H. B. Gene, *J. Neurosurg.* **2013**, *118*, 1202.
[45] W. S. Hummers, R. E. Offeman, *J. Am. Chem. Soc.* **1958**, *80*, 1339.
[46] W. C. Griffin, *J. Soc. Cosmetic Chem.* **1949**, *1*, 311.